Evaluation of different thermo-viscoplastic material models under simultaneous hot/cold forging conditions

Anton Matzenmiller, Marvin Nahrmann, Patrick Kühlmeyer

Institute of Mechanics, Department of Mechanical Engineering, University of Kassel,
Mönchebergstr. 7, 34125 Kassel, Germany

Abstract

The simultaneous hot/cold forging is an innovative metal forming process, which takes advantage of highly temperature dependent material behaviour of metallic materials. Thus, low forming forces in heated areas and high geometric accuracy in cold forged areas are achieved. The finite element analysis of such processes requires material models taking temperature and rate dependent plasticity into account. Due to the conditions of simultaneous hot/cold forging, the temperature ranges from room temperature up to nearly the melting point. The constitutive models of BAMMANN in [3] and MARIN et al. in [4], denoted as ***MAT_BAMMAN** (***MAT_51**) and ***MAT_EMMI** (***MAT_151**), are available in the material library of LS-DYNA. Both models represent the thermo-viscoplastic characteristics of metals. Furthermore, a user defined material model based on a rheological network is implemented into LS-DYNA. Each material model describes temperature dependent nonlinear isotropic and kinematic hardening, thermally activated recovery effects as well as strain rate sensitivity. In this contribution, the aforementioned thermo-viscoplastic material models are evaluated under simultaneous hot/cold forging conditions. Therefore, the material parameters are identified with the test data of the low alloy steel 50CrV4/51CrV4, the case hardening steel 16MnCr5, the low carbon steel C15 as well as the aluminium alloy AlMgSi1 by using LS-OPT. The accuracy of each model is evaluated by comparing the numerical results and test data on the basis of the mean squared error.

Keywords

simultaneous hot/cold forging, thermo-mechanical coupling, thermo-viscoplastic material models

1 Introduction

The demand for lightweight design in modern industry increases the requirements for steel and aluminium components related to mechanical properties, weight and material consumption. In addition to the material used, the production process may influence the component properties strongly. Therefore, new production methods of forming technology are developed. An innovative production process is the simultaneous hot/cold forging of a workpiece in a single step, which takes advantage of highly temperature dependent material behaviour of metals. Thus, low forming forces in heated areas and high geometric accuracy in cold forged areas are achieved. Furthermore, a process integrated heat treatment similar to press hardening leads to locally tailored material properties. Compared to a multi-step forging process or machining, the simultaneous hot/cold forming shortens production time and reduces costs.
Due to cost-intensive and time-consuming experimental tests, computer based simulations are integrated into the product development. Desirable predictions of forging simulations are the final geometry of the workpiece as well as the required forming force. Further interests are the phase transformation, the damage in the workpiece as well as thermo-mechanical fatigue of the tools. Commercial software like LS-DYNA use the finite element method (FEM) to simulate engineering problems, however, the choice of suitable material models is crucial. The finite element (FE) analysis of simultaneous hot/cold forging processes requires material models taking temperature and rate dependent plasticity into account. In this contribution, the material models ***MAT_BAMMAN** and ***MAT_EMMI** as well as the user defined constitutive model are evaluated for simultaneous hot/cold forging conditions. Each of the aforementioned thermo-viscoplastic material models includes different approaches for nonlinear isotropic and kinematic hardening, initial yield stress, strain rate sensitivity, static recovery and damage evolution. In accordance with the conditions of simultaneous hot/cold forging, the material models are investigated in the temperature range from room temperature up to nearly the melting point.

2 Motivation of a simultaneous hot/cold forging process

Due to the moderate formability of metals at room temperature, cold forging is not suitable for large degrees of forming. Hot forging as an alternative, reduces the required forming force significantly, but entails the disadvantage of low geometric accuracy. Simultaneous hot/cold forging is an innovative metal forming process combining the advantages of both forging techniques. Thereby, only a partial area of the component is heated and hot-forged, while other areas are cold-forged.
For example, the simultaneous hot/cold forging of a shaft is summarised briefly. For a more detailed description see [1,2,7,8]. The production process comprises three steps. At first, the middle of the workpiece is heated inductively up to a maximum of 1623 K (1350 °C) within twelve seconds—see Fig. 1 a). To achieve a homogeneous temperature distribution in the cross section of the heated area, a heat conduction phase is applied for five seconds, whereby the induction power is reduced strongly. After locally heating, the shaft is moved into the press and forging starts after approximately 24 seconds, whereby the temperature at the middle of the shaft is maximally 1393 K (1120 °C). As a result of the highly temperature dependent material behaviour, a significant reduction of the forming force is achieved in the heated area.
The open die forging causes a bulging of the middle part of the shaft—see Fig. 1 b). Simultaneously, the cold forging of the conical ends of the workpiece starts. After approximately three seconds, contact between the bulged material and the tools occurs, so that the final flange geometry is formed by the die—see Fig. 1 c). Finally, an integrated heat treatment, caused by rapid cooling of the hot forged area in the tool for 28 s, leads to locally tailored material properties. Thereby, a martensitic phase with high strength is induced in the flange—see [2].

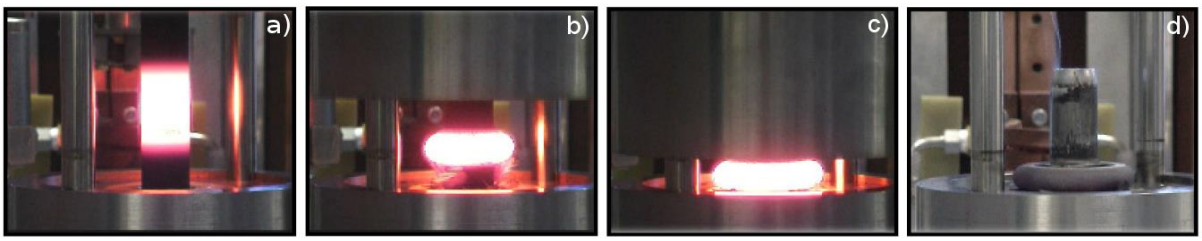

Fig.1: Simultaneous hot/cold forging of a shaft [2]

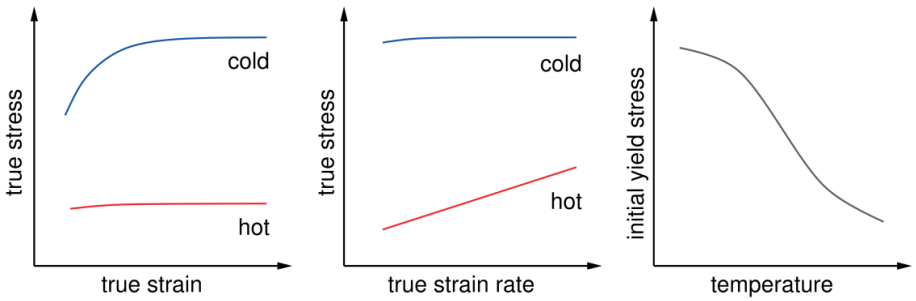

Fig.2: Schematic diagram of temperature and strain rate dependent material behaviour (according to [13]*, p. 92)*

3 Thermo-viscoplastic material models

The behaviour of metals during the forming process is strongly influenced by the process temperature and the forming speed—see Fig. 2. Metals show an extensive hardening behaviour at room temperature, whereas the hardening nearly vanishes at higher temperatures. Thereby, the hardening saturation is caused by a thermally activated recovery process. Furthermore, the strain rate dependence is mainly noticeable at high temperatures. In general, a high temperature causes a lower initial yield stress.

To model these phenomena, three different material models are analysed. The material model **`*MAT_BAMMAN (*MAT_51)`**, also known as BCJ-Model according to **B**AMMANN, **C**HIESA and **J**OHNSON presented in [3] available in LS-DYNA, represents the thermo-viscoplastic characteristics of metals. A further material model in LS-DYNA is **`*MAT_EMMI (*MAT_151)`**, denoted as **E**volving **M**icrostructural **M**odel of **I**nelasticity—see [4]. For both models, the conversion of dissipated work w_{diss} into heat is determined by means of the TAYLOR-QUINNEY approximation based on the plastic work w_{plast}—see [5].

$$w_{\mathrm{diss}} = \gamma_{\mathrm{TQ}}\, w_{\mathrm{plast}} \quad , \quad \gamma_{\mathrm{TQ}} = 0.85 \ldots 0.95 \tag{1}$$

The TAYLOR-QUINNEY coefficient γ_{TQ} is used to specify the amount of plastic work dissipated into heat and is usually chosen between 0.85 and 0.95. In addition to the aforementioned material models, a user defined thermo-viscoplasticity model is implemented into LS-DYNA by means of the keyword **`*MAT_USER_DEFINED_MATERIAL_MODEL`**—see [6,9–12]. The constitutive equations of the user material model are based on an enhanced concept of rheological models—see Fig. 3, which allows a straightforward interpretation of the material characteristic. Thereby, each rheological element is associated to energy storage or dissipation resulting in a better prediction of plastic work converted into heat—see also [10,11].

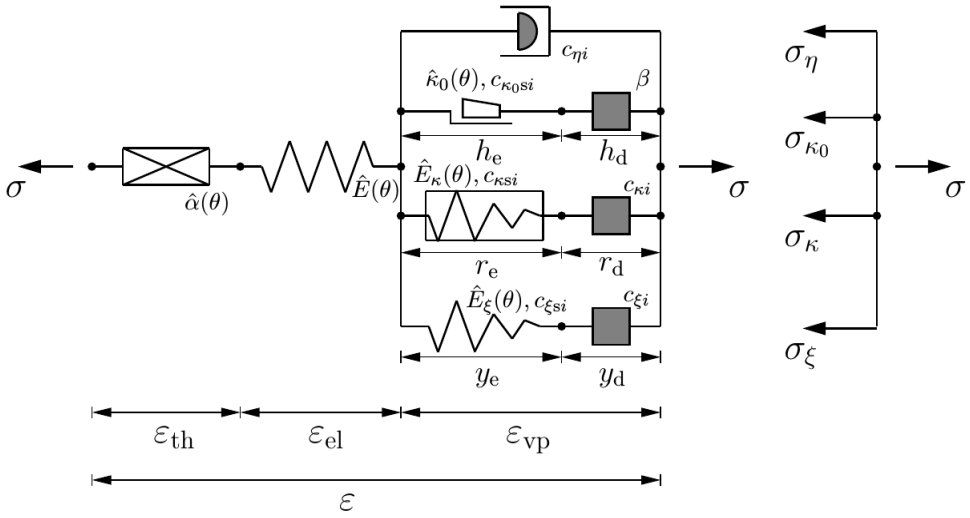

Fig.3: Rheological network of user defined material model in uniaxial case of small strains [6]

Table 1: Approaches of the initial yield stress

initial yield stress		parameters
*MAT_BAMMAN	$Y(\theta) = C_3 \exp\left(C_4/\theta\right)$	C_3, C_4
*MAT_EMMI	$\hat{\breve{Y}}(\breve{\theta}) = \dfrac{\breve{m}_1}{1+\breve{m}_2 \exp\left(-\breve{m}_3/\breve{\theta}\right)} \dfrac{1}{2}\left[1+\tanh\left(\breve{m}_4(\breve{m}_5-\breve{\theta})\right)\right]$	$\breve{m}_1, \breve{m}_2, \breve{m}_3, \breve{m}_4, \breve{m}_5$
User Model	$\hat{\kappa}_0(\theta) = \kappa_0 \dfrac{1}{2}\left(1+\tanh\left(Q_{\kappa_0}(\theta_{\kappa_0}-\theta)\right)\right)$	$\kappa_0, Q_{\kappa_0}, \theta_{\kappa_0}$

Due to the absence of test data, the material models are not used in their full abilities. Thus, the temperature dependency of the YOUNG's modulus is not considered. The kinematic hardening is neglected since no cyclic tests are available. As a consequence, the hardening behaviour is completely described by isotropic hardening. A further restriction relates to static recovery and damage evolution. As a result, only the temperature-dependent initial yield stress, the isotropic hardening as well as the strain-rate-sensitivity are considered for the three material models in this contribution.

The temperature dependency of the initial yield stress and their associated parameters is given in Tab. 1 for each of the three different material models, whereby θ is the absolute temperature in Kelvin. Moreover, the dimensionless quantities of ***MAT_EMMI** are denoted with breve symbol. For more detailed information about the non-dimensional formulation of the constitutive equations of ***MAT_EMMI** see [4]. The approach of the ***MAT_BAMMAN** model is described by the exponential function $Y(\theta)$ with two parameters, whereas the ***MAT_EMMI** option $\hat{\breve{Y}}(\breve{\theta})$ combines an inverse exponential function with the hyperbolic tangent and five parameters. For the initial yield stress $\hat{\kappa}_0(\theta)$ of the user defined material model, the hyperbolic tangent is used with three parameters and consequently is a special case of the approach in ***MAT_EMMI** for $\breve{m}_2 = 0$.

The approaches of the isotropic hardening and their associated parameters are given in Tab. 2 for each material model. Here, the effective viscoplastic strain is denoted as $\bar{\mathrm{E}}_{\mathrm{vp}}$. Each material model consists of isotropic hardening assumption with a hardening modulus and a saturation term. The hardening assumption of ***MAT_BAMMAN** is described by the exponential decay function $H(\theta)$ and the inverse exponential saturation function $R_{\mathrm{d}}(\theta)$, whereby a total of four parameters are necessary. The isotropic hardening approach of ***MAT_EMMI** includes the constant hardening modulus $\breve{H}$ and the temperature-dependent saturation function $\breve{R}_{\mathrm{D}}(\breve{\theta})$, whereby an inverse exponential function is taken analogously to ***MAT_BAMMAN** with an overall of three parameters. For the user model, the temperature-dependent hardening function $\hat{E}_\kappa(\theta)$ and a constant saturation parameter $\varepsilon_\kappa^\infty$ is taken into account, whereby a hyperbolic tangent is chosen for the temperature-dependent hardening function $\hat{E}_\kappa(\theta)$. This requires a total of four parameters.

The approaches of the strain rate sensitivity and their associated parameters are given in Tab. 3 for each of the three material models. Here, the plastic multiplier is denoted as λ and the yield function as F. Each investigated material model uses a PERZYNA viscoplasticity approach to represent the strain rate sensitivity. While a pure hyperbolic sine function is used with ***MAT_BAMMAN**, the exponent $\breve{n}(\breve{\theta})$ is additionally introduced with ***MAT_EMMI**. In the user model, the exponent $\hat{m}(\theta)$, which is a function of

Table 2: Approaches of the isotropic hardening

isotropic hardening		parameters
*MAT_BAMMAN	$\dot{\kappa} = \left(H(\theta) - R_{\mathrm{d}}(\theta)\kappa^2\right)\dot{\bar{\mathrm{E}}}_{\mathrm{vp}}$ $H(\theta) = C_{15}\exp\left(C_{16}/\theta\right) \quad , \quad R_{\mathrm{d}}(\theta) = C_{13}\exp\left(-C_{14}/\theta\right)$	$C_{13}, C_{14}, C_{15}, C_{16}$
*MAT_EMMI	$\overset{*}{\breve{\kappa}} = \left(\breve{H} - \breve{R}_{\mathrm{D}}(\breve{\theta})\,\breve{\kappa}\right)\overset{*}{\bar{\mathrm{E}}}_{\mathrm{vp}}$ $\breve{H} = \breve{c}_6 \quad , \quad \breve{R}_{\mathrm{D}}(\breve{\theta}) = \breve{c}_5\exp\left(-\breve{Q}_3/\breve{\theta}\right)$	$\breve{c}_5, \breve{c}_6, \breve{Q}_3$
User Model	$\dot{\kappa} = \left(\hat{E}_\kappa(\theta) - \dfrac{\kappa}{\varepsilon_\kappa^\infty}\right)\dot{\bar{\mathrm{E}}}_{\mathrm{vp}} + \dfrac{\partial_\theta \hat{E}_\kappa(\theta)}{\hat{E}_\kappa(\theta)}\,\kappa\,\dot{\theta}$ $\hat{E}_\kappa(\theta) = \dfrac{1}{2}E_\kappa\left(1+\tanh\left(Q_\kappa(\theta_\kappa-\theta)\right)\right)$	$E_\kappa, Q_\kappa, \theta_\kappa, \varepsilon_\kappa^\infty$

Table 3: Approaches of the strain rate sensitivity

strain rate sensitivity		parameters
*MAT_BAMMAN	$\lambda = f(\theta)\,\sinh\left[\frac{F}{V(\theta)}\right]$ $f(\theta) = C_5\,\exp\left(-C_6/\theta\right) \quad , \quad V(\theta) = C_1\,\exp\left(-C_2/\theta\right)$	C_1, C_2, C_5, C_6
*MAT_EMMI	$\lambda = \breve{f}(\breve{\theta})\left[\sinh\left(\left\langle\frac{\breve{F}}{\breve{\kappa}+\breve{Y}(\breve{\theta})}\right\rangle\right)\right]^{\breve{n}(\breve{\theta})}$ $\breve{f}(\breve{\theta}) = \breve{c}_2\,\exp\left(\frac{-\breve{Q}_1}{\breve{\theta}}\right) \quad , \quad \breve{n}(\breve{\theta}) = \frac{\breve{c}_9}{\breve{\theta}} + \breve{c}_1$	$\breve{c}_1, \breve{c}_2, \breve{c}_9, \breve{Q}_1$
User Model	$\lambda = \frac{1}{\hat{\eta}(\theta)}\left\langle\frac{F}{\hat{D}(\kappa,\theta)}\right\rangle^{\hat{m}(\theta)} \quad , \quad \hat{D}(\kappa,\theta) := D_0 + D_1(\hat{\kappa}_0(\theta)+\kappa)$ $\hat{\eta}(\theta) = \eta\,\exp\left(Q_\eta/\theta\right) \quad , \quad \hat{m}(\theta) = m_0 + \frac{m_1}{\theta}$	η, Q_η, m_0, m_1

temperature, represents the temperature dependency of the plastic multiplier. Each material model has a temperature-dependent pre-factor $\hat{\eta}(\theta)$ respectively $f(\theta)/\breve{f}(\breve{\theta})$, which can be interpreted as pseudo-viscosity for the user model and as pseudo-fluidity for ***MAT_BAMMAN** and ***MAT_EMMI**. The denominator $V(\theta)$ within the hyperbolic sine function of ***MAT_BAMMAN** is represented by a temperature-dependent exponential function as the so-called drag-stress. The approach of ***MAT_EMMI** consists of the isotropic hardening and the initial yield stress as drag-stress. This approach can be achieved in the user model by setting D_0 = 0 and D_1 = 1. In this contribution, the parameters D_0 = 10^6 N/m^2 and D_1 = 0 are chosen, whereby only the stress unit disappears and thus no drag-stress is active.

4 Identification of model parameters

The presented approaches of each material model contain various functions to describe the temperature and strain rate dependent material behaviour, for which a certain number of parameters have to be determined. Therefore, test data of various metals are taken into account for different strain rates and temperatures. The experimental data of the case hardening steel 16MnCr5 as well as the low carbon steel C15 are given in [13] with the true strain rate of 1.6 1/s, 8.0 1/s as well as 40.0 1/s. Hereby, the temperature ranges from 293 K (20 °C) up to 1373 K (1100 °C) in case of 16MnCr5, respectively from 293 K (20 °C) up to 1473 K (1200 °C) in case of C15. Furthermore, test data of the aluminium alloy AlMgSi1 is given in [13] within a temperature range from 573 K (300 °C) to 773 K (500 °C) at the true strain rates of 0.3 1/s, 3.0 1/s and 100 1/s. It should be mentioned that the temperature range is only given for hot forming here. Test data of the low alloy steel 50CrV4 is given in [14] within a temperature range from 1073 K (800 °C) to 1423 K (1150 °C) at the true strain rates between 0.001 1/s and 10.0 1/s. For the nearly similar material 51CrV4, experimental data for temperatures from 273 K (20 °C) to 973 K (700 °C) are given in [15] at the engineering strain rate of 0.025 1/s. It is assumed that both materials 50CrV4 and 51CrV4 have nearly the same mechanical properties and therefore can be used equivalently for the identification process.
The test data of 16MnCr5, C15, AlMgSi1 as well as 50CrV4 are generated by upsetting tests to achieve large degrees of forming. In contrast to the other test data, 51CrV4 is measured by tensile testing. Thereby, necking occurs in the middle of the specimen resulting in an early rupture. Hence, only small deformations are obtained by tensile testing. To achieve a homogenous stress state, the tensile test data is only applied before necking of the specimen occurs.
The fitting process of the simulation to the test data is done by using the optimisation tool LS-OPT. The deviation between the measured and simulated flow curves is investigated on the basis of the mean squared error (MSE)

$$\epsilon_{\mathrm{MSE}} = \frac{1}{n}\sum_{i=1}^{n}\left(\frac{\hat{Y}_i - Y_i}{S_i}\right)^2 \quad , \tag{2}$$

which is calculated and minimised during the optimisation process. Here, $\hat{Y}_i$ relates to the simulation value, Y_i to the experimental value and S_i is a scaling factor, which is determined from the maximum

experimental value. Furthermore, n is the total number of data pairs. Due to the large amount of test data, flow curves at certain temperatures and strain rates are selected for the optimisation process, whereby the parameters are identified simultaneously.
For simplicity, a single eight-node solid element (**ELFORM=2**) with initial edge lengths of L_0 = 10 mm is used for the FE simulation. The displacement controlled loading is applied at all nodes of the upper element side. The degrees of freedom of the lower nodes are restraint in order to generate a uniaxial stress state due to tensile and pressure load. For simulating the tensile test, the displacements $u(t) = L_0\ \dot{\varepsilon}_{\mathrm{eng}}\ t$ are prescribed linearly over time t such that the engineering strain rate $\dot{\varepsilon}_{\mathrm{eng}} = \dot{u}(t)/L_0$ is kept constant. To simulate the compression test, the true strain rate $\dot{\varepsilon}_{\mathrm{true}} = \dot{u}(t)/L(t)$ is prescribed as a constant value. The resulting time-displacement function is determined by means of the relation between engineering and true strain $\varepsilon_{\mathrm{true}} = \ln(1+\varepsilon_{\mathrm{eng}})$ that leads to $\dot{\varepsilon}_{\mathrm{true}} = \dot{\varepsilon}_{\mathrm{eng}}/(1+\varepsilon_{\mathrm{eng}})$. Finally, the resulting nonlinear time-displacement function is given with $u(t) = L_0\ (\exp(\dot{\varepsilon}_{\mathrm{true}}\ t) - 1\ )$.
During forging processes, the mutual interactions of the displacement and temperature field is caused by the thermo-mechanical coupling. To solve the thermo-mechanical coupled problem, the staggered solution scheme is used in LS-DYNA. Thereby, the mechanical problem is implicitly solved with fixed temperatures and the thermal problem is implicitly solved with fixed displacements. The thermal and mechanical time step size is chosen identically to achieve a high temporal resolution. The finally identified material parameters of ***MAT_BAMMAN**, ***MAT_EMMI** and the User Model for each investigated metal are summarised in Tab. 5—see appendix.

5 Evaluation of material models

The agreement of simulation results with experimental data is an essential criterion for the use of a material model. The accuracy of each aforementioned model is evaluated by comparing the numerical results and test data on the basis of the MSE according to Eq. (2). The simulation results are presented with positive stress and strain to correspond with the experimental data base, even if a compressive load is applied.
The predicted flow curves of ***MAT_BAMMAN**, ***MAT_EMMI** and the User Model are compared to the experimental data of the case hardening steel 16MnCr5 at the true strain rate 1.6 1/s in Fig. 4. The test data at 293 K as well as at 1373 K is in good agreement with the prediction of ***MAT_BAMMAN**. However, the region in between is insufficiently described, so that ***MAT_BAMMAN** is not suitable for the entire temperature range. The experimental data in the entire range of temperature is well represented by ***MAT_EMMI**. However, the hardening cannot be predicted very well at 293 K since no temperature dependent hardening modulus is used—see Tab. 2. The User Model shows a very good agreement with the experimental data over the entire range of temperature. In contrast to ***MAT_EMMI**, the hardening can be described better at low temperatures.
The comparison between the simulation results with ***MAT_BAMMAN**, ***MAT_EMMI** as well as the User Model and the test data of the low carbon steel C15 at the true strain rate of 1.6 1/s is shown in Fig. 5. The test data at 293 K and 1473 K are acceptably captured by ***MAT_BAMMAN**. However, the temperature range in between is described poorly. A good agreement between experimental data and simulation results is achieved with ***MAT_EMMI** at the temperatures 273 K as well as from 773 K up to

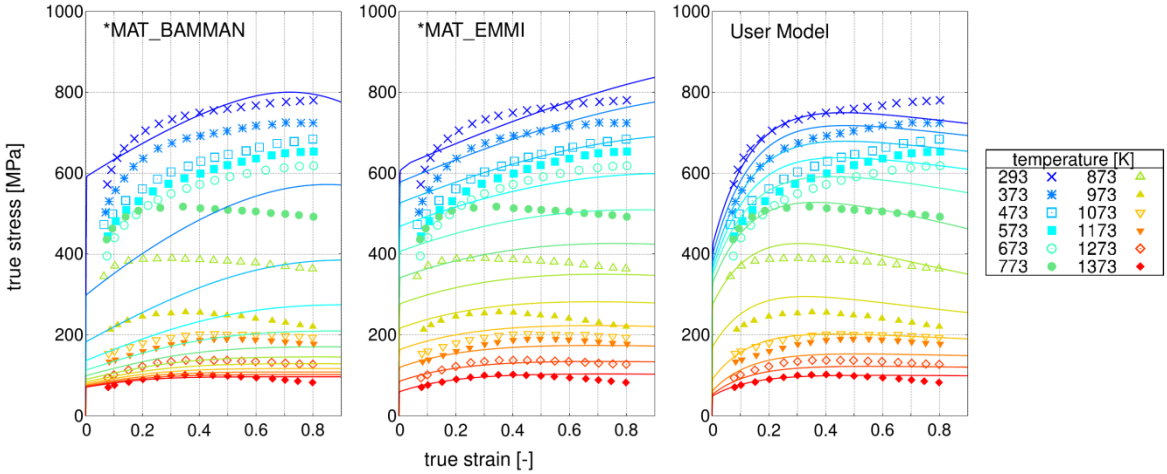

Fig.4: Test data (dots) and simulation results (lines) of 16MnCr5 at true strain rate 1.6 1/s

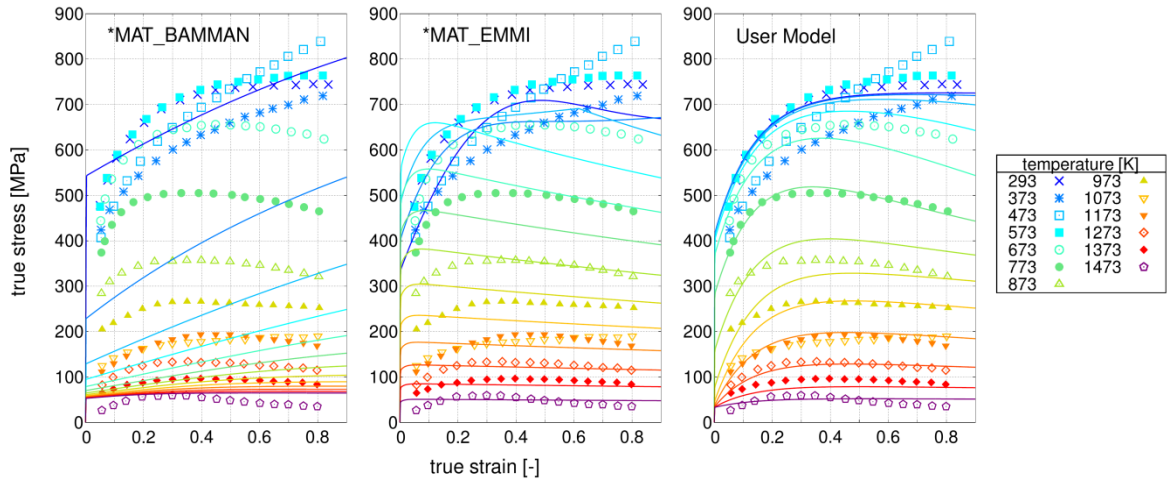

Fig.5: Test data (dots) and simulation results (lines) of C15 at true strain rate 1.6 1/s

1473 K. The User Model captures the test data even better at the aforementioned temperatures. However, there is a strong deviation between test and simulation data in the range of 373 K–673 K, where the decrease of flow stress is interrupted in the test data. The reason of interruption is the so called blue brittleness, which occurs for this steel type with the characteristic blue colour at approximately 473 K–673 K. Within this temperature range, nitrogen atoms diffuse into dislocation regions and thereby block dislocation motions leading to increasing flow stress. Due to an empirical yield stress approach, none of the investigated material models can predict the blue brittleness at all.

The simulation results of ***MAT_BAMMAN**, ***MAT_EMMI** as well as the User Model are compared to the test data of the low alloy steel 51CrV4 at the engineering strain rate 0.025 1/s and temperatures from 293 K to 973 K in Fig. 6. Simulation and test data of 50CrV4 are compared at temperatures from 1073 K to 1423 K at the true strain rate 0.1 1/s in Fig. 7. The test data at 293 K and at 1423 K are in good agreement with the simulation using ***MAT_BAMMAN**. Due to the exponential approach for the initial yield stress, the region in between is insufficiently reproduced. Therefore, ***MAT_BAMMAN** is not suitable in the entire temperature range. The experimental data over the entire temperature range is represented well by ***MAT_EMMI**. However, the hardening at low temperatures is not predicted precisely since no temperature dependent hardening modulus is used—see Tab. 2. The User Model shows a very good agreement with the experimental data over the entire range of temperature. In contrast to ***MAT_EMMI**, the hardening at low temperatures is captured more accurately by the User Model.

The comparison of the simulation results with ***MAT_BAMMAN**, ***MAT_EMMI** as well as the User Model with the test data of the aluminium alloy AlMgSi1 at true strain rate of 0.3 1/s is shown in Fig. 8. The experimental data is reproduced acceptably over the entire range of temperature by ***MAT_BAMMAN**. However, the hardening behaviour is too strong compared to test data. Nevertheless, ***MAT_BAMMAN** is a suitable model to predict the material behaviour of AlMgSi1. A good agreement of simulation and

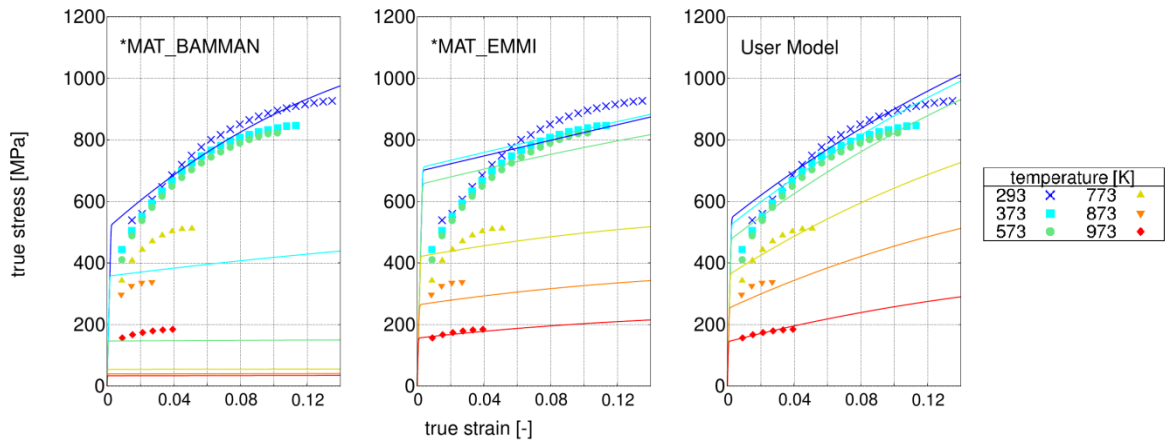

Fig.6: Test data (dots) and simulation results (lines) of 51CrV4 at engineering strain rate 0.025 1/s

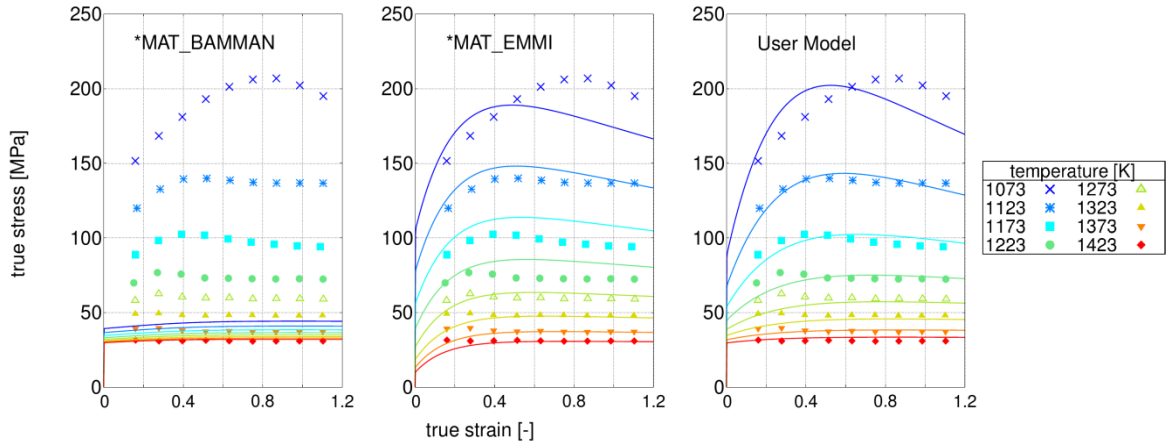

Fig.7: Test data (dots) and simulation results (lines) of 50CrV4 at true strain rate 0.1 1/s

experimental data is achieved by ***MAT_EMMI** as well as the User Model.
For the evaluation of the material models, the averaged MSE values are compared in Tab. 4. Thereby, the MSE is determined for each load case and averaged to a single value, whereby a load case contains a specific temperature and strain rate. As a result, the MSE values of ***MAT_BAMMAN** are the highest ones in all cases. Therefore, this material model is least suitable to describe the investigated material behaviour. The material model ***MAT_EMMI** provides significant better results than ***MAT_BAMMAN** and causes a lower MSE of approximately one order of magnitude. Consequently, the ***MAT_EMMI** is a suitable model to represent the characteristics of metals within the complete temperature range. The simulation results with the User Model have the lowest MSE values and therefore the User Model is the most suitable material model.
Comparing the MSE values of the User Model and ***MAT_EMMI**, the User Model improves the prediction accuracy about 9 % for 16MnCr5 and 17 % for C15. The improvement for 50CrV4/51CrV4 is even 63 % respectively 15 % for AlMgSi1.
In view of the poor accuracy of ***MAT_BAMMAN**, the effort for the identification of ten parameters is very high. The, ***MAT_EMMI** model uses twelve parameters in total and produces significant better simulation results. Although the User Model only needs eleven parameters, the accuracy of simulation results with the test data is even higher than with ***MAT_EMMI**.

Table 4: Overall MSE values (in 10^{-3}) of investigated metals and material models

	*MAT_BAMMAN	*MAT_EMMI	User Model
16MnCr5	876.33	8.04	7.29
C15	197.97	17.98	14.94
(50/51)CrV4	210.91	12.90	4.76
AlMgSi1	27.71	3.06	2.61

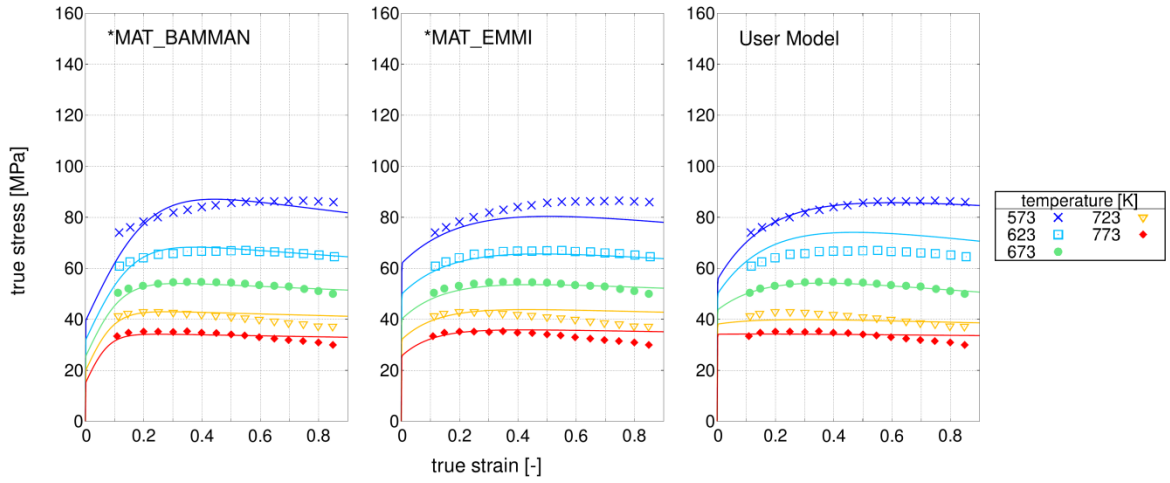

Fig.8: Test data (dots) and simulation results (lines) of AlMgSi1 at true strain rate 0.3 1/s

6 Summary

The thermo-viscoplastic material models ***MAT_BAMMAN (*MAT_51)**, ***MAT_EMMI (*MAT_151)** and the user defined material model are investigated under simultaneous hot/cold forging conditions. Approaches of each model for the initial yield stress, the isotropic hardening as well as the strain rate sensitivity are presented and discussed. The model parameters are identified by fitting the simulation results to test data of the case hardening steel 16MnCr5, the low carbon steel C15, the low alloy steel 50CrV4/51CrV4 and the aluminium alloy AlMgSi1 by using LS-OPT. Each of the aforementioned material models is evaluated by means of a comparison between simulation result and test data based on the MSE. As a result of the evaluation, the test data in the entire temperature range is not predicted suitably by ***MAT_BAMMAN**. The prediction of ***MAT_EMMI** leads to a satisfactory agreement with the test data in the entire temperature range. However, the best agreement with the applied test data is predicted by the User Model.

Acknowledgements

The authors thankfully acknowledge the financial support of the German Research Foundation (DFG) through grant no. Ma1186/5-2.

References

[1] Steinhoff, K., Maier, H. and Biermann, D. (editors): "Functionally graded materials in industrial mass production", Verlag Wissenschaftliche Scripten, Auerbach, 2009

[2] Weidig, U., Hübner, K. and Steinhoff, K.: "Bulk steel products with functionally graded properties produced by differential thermo-mechanical processing", Steel Research Int., vol. 79, 2008, pp. 59–65

[3] Bammann, D.J.: "Modeling temperature and strain rate dependent large deformations of metals", Appl. Mech. Rev., vol. 43, 1990, pp. 312–319

[4] Marin, E.B., Bammann, D.J., Regueiro, R.A. and Johnson, G.C.: "On the Formulation, Parameter Identification and Numerical Integration of the EMMI Model: Plasticity and Isotropic Damage", Sandia Report SAND2006-0200, Sandia National Laboratories, California, USA, 2006, URL: http://prod.sandia.gov/techlib/access-control.cgi/2006/060200.pdf

[5] Taylor, G. I. and Quinney, H.: "The latent energy remaining in a metal after cold working". Proceedings of the Royal Society of London, A: Mathematical, Physical and Engineering Sciences, vol. 143, 1934, pp. 307–326.

[6] Bröcker, C. and Matzenmiller, A.: A thermoviscoplastic model with damage for simultaneous hot/cold forging analysis, In: E. Onate, D. Owen, D.Peric und B. Suarez: "Proceedings of 12th International Conference on Computational Plasticity – Fundamentals and Applications" (COMPLAS XII), International Center for Numerical Methods in Engineering (CIMNE), Barcelona, Spain, 2013, URL: http://www.ifm.maschinenbau.uni-kassel.de/%7Eamat/publikationen/oeffentlich/Broecker-A_THERMOVISCOPLASTIC_MODEL_WITH_DAMAGE_FOR_SIMULTANEOUS_HOT%E2%81%84COLD_FORGING_ANALYSIS.pdf

[7] Matzenmiller, A. and Bröcker, C.: "Thermo-mechanically coupled FE analysis and sensitivity study of simultaneous hot/cold forging process with local inductive heating and cooling", Int J Mater Form, vol. 5, 2012, pp. 275–300

[8] Matzenmiller, A., Bröcker, C. and Gerlach, S.: "FE-Analysis of Simultaneous Hot/Cold Forging", Steel Research Int., vol. 80, 2009, pp. 130–136

[9] Bröcker, C. and Matzenmiller, A.: "On the generalization of uniaxial thermoviscoplasticity with damage to finite deformations based on enhanced rheological models", Technische Mechanik, vol. 34, 2014, pp. 142-165

[10] Bröcker, C. and Matzenmiller, A.: "An enhanced concept of rheological models to represent nonlinear thermoviscoplasticity and its energy storage behaviour". Continuum Mechanics and Thermodynamics, vol. 25, 2013, pp. 749–778.

[11] Bröcker, C. and Matzenmiller, A.: "An enhanced concept of rheological models to represent nonlinear thermoviscoplasticity and its energy storage behavior, part 2: spatial generalization for small strains". Continuum Mechanics and Thermodynamics, vol. 27, 2015, pp. 325–347.

[12] Szczepaniak, A., Bröcker, C. and Matzenmiller, A.: "Implementierung eines Thermoviskoplastizitäts-modells mit Schädigung für die simultane Kalt-/Warmumformung", LS-DYNA Forum, Bamberg, 2014

[13] Doege, E. and Behrens, B.-A.: "Handbuch Umformtechnik - Grundlagen, Technologien, Maschinen", Springer, Berlin, 2010

[14] Hagen, M.: "Werkstoffmodelle zur thermomechanischen Behandlung des Stahls 50CrV4", Ph.D. Thesis, Faculty of Mining, Metallurgy, and Geosciences, RWTH Aachen University, 1990
[15] Scholtes, B.: Personal communication. University of Kassel, Department of Mechanical Engineering, Institute of Material Science, Mönchebergstr. 3, 34125 Kassel, 2009

Appendix

Table 5: Identified parameters of the investigated material models

		16MnCr5	C15	(50/51)CrV4	AlMgSi1
*MAT_BAMMAN: initial yield stress					
C_3	[N/m²]	1.7004 10^7	4.7033 10^6	2.4738 10^7	3.8078 10^4
C_4	[K]	1.0205 10^3	1.3629 10^3	1.2151 10^2	2.5661 10^{-5}
*MAT_BAMMAN: isotropic hardening					
C_{13}	[m²/N]	1.5467 10^{-6}	3.7854 10^{-5}	7.0609 10^{-5}	1.9986 10^{-4}
C_{14}	[K]	3.1400 10^3	6.8995 10^3	5.7402 10^3	4.4629 10^3
C_{15}	[N/m²]	5.4853 10^7	2.3658 10^7	1.2467 10^6	2.2665 10^8
C_{16}	[K]	9.5639 10^2	1.2071 10^3	2.4440 10^3	4.5834 10^1
*MAT_BAMMAN: strain rate sensitivity					
C_1	[N/m²]	2.3445 10^7	5.4241 10^6	3.6272 10^7	6.1235 10^6
C_2	[K]	1.1769 10^{-3}	4.9720 10^{-3}	2.1549 10^0	9.5004 10^{-2}
C_5	[1/s]	7.7219 10^{-1}	2.3260 10^{-3}	9.6919 10^1	4.8469 10^3
C_6	[K]	1.9439 10^1	5.0000 10^2	6.1680 10^3	8.8351 10^3
*MAT_EMMI: initial yield stress					
$\breve{m}_1$	[-]	2.2039 10^{-3}	2.0614 10^{-4}	4.7359 10^{-4}	5.0753 10^{-3}
$\breve{m}_2$	[-]	1.5474 10^0	1.8729 10^1	5.5639 10^{-2}	4.8819 10^{-2}
$\breve{m}_3$	[-]	1.0657 10^{-4}	2.4278 10^0	3.5037 10^{-2}	4.0010 10^0
$\breve{m}_4$	[-]	3.3609 10^0	8.0903 10^0	3.1355 10^0	1.8999 10^0
$\breve{m}_5$	[-]	4.8292 10^{-1}	9.5687 10^{-1}	4.5232 10^{-1}	2.7153 10^{-3}
*MAT_EMMI: isotropic hardening					
$\breve{c}_5$	[-]	2.5853 10^1	1.5349 10^2	1.7335 10^1	6.8426 10^{-2}
$\breve{c}_6$	[-]	4.7002 10^{-4}	1.0311 10^{-3}	7.0219 10^{-4}	8.7748 10^{-4}
$\breve{Q}_3$	[-]	1.2826 10^0	6.2111 10^{-1}	7.5213 10^{-1}	1.6437 10^0
*MAT_EMMI: strain rate sensitivity					
$\breve{c}_1$	[-]	1.4447 10^{-2}	2.0296 10^{-1}	1.2803 10^0	1.3858 10^{-2}
$\breve{c}_2$	[-]	1.0004 10^{-5}	1.3333 10^{-1}	9.1369 10^1	5.1449 10^{-7}
$\breve{c}_9$	[-]	1.1418 10^0	3.9766 10^{-1}	1.0001 10^{-1}	2.3568 10^0
$\breve{Q}_1$	[-]	4.1991 10^0	1.1109 10^1	1.5995 10^1	4.3542 10^0
User Model: initial yield stress					
κ_0	[N/m²]	2.7062 10^8	3.8056 10^8	4.4213 10^8	1.7211 10^7
Q_{κ_0}	[1/K]	7.9930 10^{-3}	6.8182 10^{-3}	5.1701 10^{-3}	9.3016 10^{-3}
θ_{κ_0}	[K]	9.4798 10^2	8.1849 10^2	8.7280 10^2	6.5469 10^2
User Model: isotropic hardening					
E_κ	[N/m²]	3.1017 10^9	2.3334 10^9	4.4210 10^9	2.0455 10^8
Q_κ	[1/K]	1.8797 10^{-3}	4.9547 10^{-3}	5.4023 10^{-3}	2.0780 10^{-2}
θ_κ	[K]	8.6949 10^2	1.2060 10^3	9.0657 10^2	6.6815 10^2
$\varepsilon_\kappa^\infty$	[-]	1.3488 10^{-1}	1.3370 10^{-1}	2.8388 10^{-1}	1.6854 10^{-1}
User Model: strain rate sensitivity					
η	[s]	3.6961 10^2	2.5912 10^2	9.5135 10^1	2.0493 10^1
Q_η	[K]	7.2394 10^3	3.7554 10^3	1.0798 10^4	1.9705 10^4
m_0	[-]	2.1947 10^0	1.8214 10^0	1.6842 10^0	2.5437 10^0
m_1	[K]	1.1852 10^3	1.0149 10^3	1.8859 10^3	4.1466 10^3